

# Single-cycle terawatt twisted-light pulses at midinfrared wavelengths above 10 $\mu$ m

## Authors:

Xing-Long Zhu<sup>1,2,3</sup>, Min Chen<sup>1,3\*</sup>, Su-Ming Weng<sup>1,3</sup>, Paul McKenna<sup>2,4</sup>, Zheng-Ming Sheng<sup>1,2,3,4,5\*</sup>, and Jie Zhang<sup>1,3,6</sup>

## Affiliations:

<sup>1</sup> Key Laboratory for Laser Plasmas (MOE), School of Physics and Astronomy, Shanghai Jiao Tong University, Shanghai 200240, China

<sup>2</sup> SUPA, Department of Physics, University of Strathclyde, Glasgow G4 0NG, UK

<sup>3</sup> Collaborative Innovation Center of IFSA, Shanghai Jiao Tong University, Shanghai 200240, China

<sup>4</sup> Cockcroft Institute, Sci-Tech Daresbury, Cheshire WA4 4AD, UK

<sup>5</sup> Tsung-Dao Lee Institute, Shanghai 200240, China

<sup>6</sup> Institute of Physics, Chinese Academy of Sciences, Beijing 100190, China

\*Corresponding author. Email: minchen@sjtu.edu.cn (M.C.); z.sheng@strath.ac.uk (Z.M.S.)

Twisted light beams with orbital angular momentum provide an additional degree of freedom in controlling light-matter interactions, which are interesting for fundamental and applied research. Although there are various methods that can produce twisted laser beams at sub-micrometer or shorter wavelengths, it is still challenging to extend such beams to mid-infrared (mid-IR) wavelengths with relativistic intensity. Here, we present a promising scheme to generate such pulses converted through frequency downshift of intense driver optical pulses via a plasma-based photon decelerator. The resulting near-single-cycle vortex pulses cover a broad mid-IR spectral range up to 18  $\mu$ m with energy conversion efficiency of 4.8% (energy  $\sim$ 150mJ) in the wavelength range above 7  $\mu$ m. This long-wavelength infrared pulses at the terawatt level can be focused to relativistically high intensity, which may offer significant opportunities for high-field physics and ultrafast applications.

## I. Introduction

Twisted light beams carrying orbital angular momentum (OAM) exhibit typical screw-like spatial and phase structures, called ‘optical vortices’, which are associated with Laguerre-Gaussian (LG) modes and characterized by the vortex topological charge. The OAM of light first recognized by Allen *et al.* in 1992 [1] has found a wide range of applications in diverse research disciplines, including quantum information science [2,3], microscopy [4], optical manipulation [5], biology [6], and even astrophysics [7]. In recent years, significant progress has been made in the development of such light sources [8]. Twisted light beams with wavelengths of near-infrared, visible and extreme ultraviolet have been produced [9-12] through optical mode converters such as cylindrical lenses, spiral phase plates and phase fork gratings. However, these techniques are not suitable for creating high-intensity laser pulses at long wavelengths beyond a few micrometers. The high-intensity laser pulses can potentially push light-matter interactions into the relativistic regime and even quantum electrodynamics [13-15]. Currently, high-power intense mid-infrared (mid-IR) pulses are highly desired for many scientific studies [16-18], including bright high-harmonic generation [19,20], time-resolved infrared spectroscopy [21], ultrafast imaging of molecular dynamics [22], etc. These applications would benefit from the long wavelength ( $\lambda$ ), ultrashort pulse duration and high intensity ( $I_0$ ) of the driving electromagnetic fields, which may lead to shorter and brighter attosecond light pulses with higher photon energy ( $\propto I_0\lambda^2$ ) [19,20]. The development of high-intensity twisted light sources in the mid-IR region would combine the advantages of twisted light beams and intense mid-IR pulses. In particular, these pulses with tunable long wavelength, few-cycle duration, and controlled carrier-envelope phase (CEP) are very useful for ultrafast science [23] and high-field physics [24,25]. However, due to various limitations in optical materials and elements such as wavelength coverage limit for amplification or optical breakdown, it is challenging to generate high-intensity few-cycle long-wavelength light pulses with current techniques.

To solve these problems, we propose a scheme to generate terawatt (TW)-class, hundred-millijoule (mJ), near-single-cycle twisted light pulses via a plasma-based photon decelerator driven by a LG laser pulse in underdense plasma. In this scheme, the pulse frequency is tunable at a broad mid-IR spectral coverage, and its CEP and topological structure are also controllable with laser and plasma parameters. Such intense pulses, with high peak power, broad infrared spectrum, vortex structure, and near single-cycle duration, are extremely useful for a variety of scientific applications.

## II. Scheme and Theory for Photon Frequency Modulation

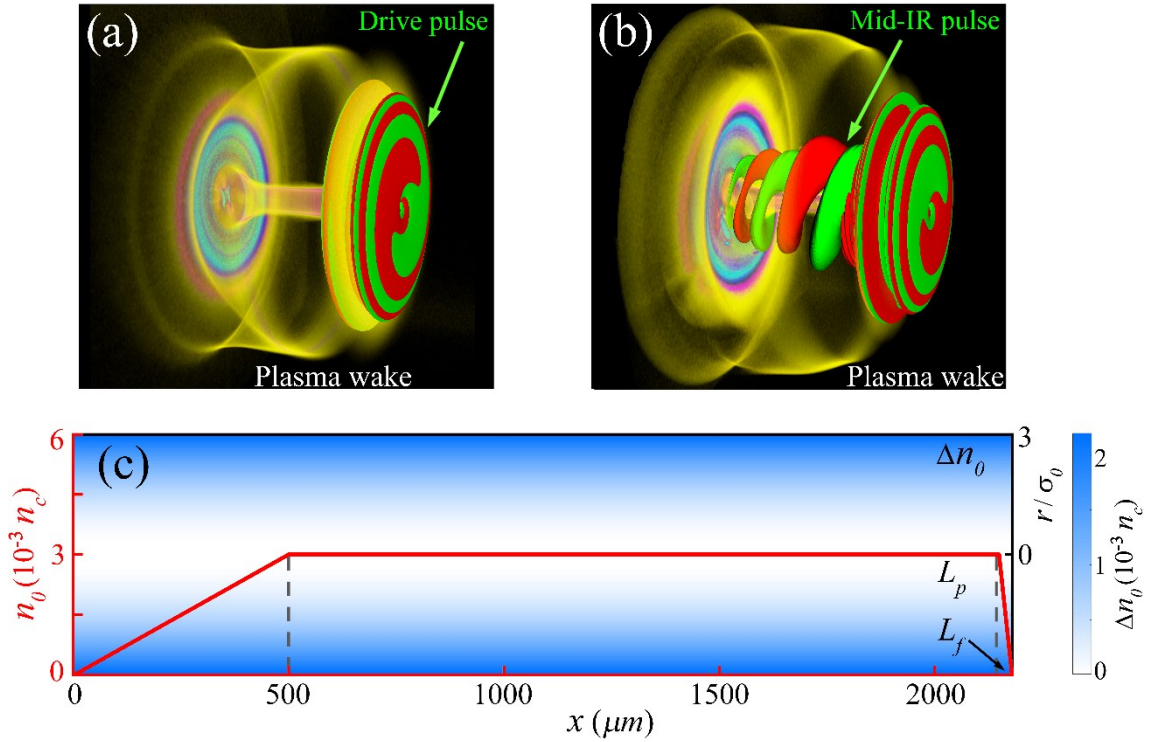


**FIG. 1.** Schematic of the plasma photon decelerator for producing intense mid-IR vortex pulses. (a) A plasma wake with a bubble-like shape is created during the propagation of an intense laser pulse in an underdense plasma channel. (b) An intense mid-IR, few-cycle pulse is generated inside the bubble, behind the drive laser pulse, after a propagation distance of 2mm, when it undergoes strong frequency downshift. (c) The density distribution of the plasma channel, where the density is set to  $n_{e0} = n_0 + \Delta n_0$ , the red line indicates the background density profile along the  $x$ -axis with  $n_0 = 3 \times 10^{-3} n_c$  at the plateau, the color map represents the channel depth of  $\Delta n_0 = (\pi r_e \sigma_0^2)^{-1} (r^2 / \sigma_0^2)$ ,  $r$  is the distance from the channel axis,  $r_e = e^2 / m_e c^2$  is the classical electron radius,  $\sigma_0 = 20 \mu\text{m}$  is the laser spot size, and  $n_c = m_e \omega_0^2 / 4\pi e^2 = 1.1 \times 10^{21} \text{cm}^{-3}$  is the critical plasma density.  $L_p$  and  $L_f$  represents the longitudinal length of the

density plateau and down-ramp, respectively.

Figure 1 presents the schematic diagram of our mechanism, in which an ultrashort intense LG laser pulse propagates in underdense plasma and drives a wake [Fig. 1(a)]. This pulse experiences strong and continuous frequency downshift (so-called ‘photon deceleration’) due to the group velocity dispersion and phase modulation by the wake excitation. The decelerated photons are trapped and accumulate inside the wake bubble, where their frequency can be as low as the plasma frequency, i.e., in the mid-IR regime. The spatial and temporal structures of the mid-IR pulse resemble the drive laser pulse, as shown in Fig. 1(b). A plasma channel as shown in Fig. 1(c) is adopted in order to guide and confine efficiently the laser pulse propagation in plasma over much longer than its diffraction length [26,27]. The longitudinal density profile is trapezoidal, where the lengths of the plateau and down-ramp play important roles in the mid-IR pulse generation as discussed later.

In the following, we describe the basic physical mechanism for frequency downshift. It is well-known that a laser pulse can be modulated as it propagates in plasma, which can lead to frequency shifts, temporal shaping or compression of laser pulses [28-32]. The interaction of intense laser pulses with tenuous plasma can be described by the following coupled equations [33-36]:  $\left(\frac{2}{c} \frac{\partial}{\partial \xi} - \frac{1}{c^2} \frac{\partial}{\partial \tau}\right) \frac{\partial \mathbf{a}}{\partial \tau} = k_p^2 \frac{\mathbf{a}}{1+\phi}$  and  $\frac{\partial^2 \phi}{\partial \xi^2} = \frac{k_p^2}{2} \left[ \frac{1+a^2}{(1+\phi)^2} - 1 \right]$ , where  $\xi = x - ct$ ,  $\tau = t$ ,  $k_p = \frac{\omega_p}{c}$ ,  $\phi = \frac{e\Phi}{m_e c^2}$  and  $\mathbf{a} = \frac{e\mathbf{A}}{m_e c^2}$  are the normalized scalar and vector potentials associated with the wakefields and the laser pulse, respectively,  $\omega_p = \sqrt{\frac{4\pi n_e e^2}{m_e}}$  is the plasma frequency,  $e$  is the unit charge, and  $m_e$  is the electron mass. The excitation of laser wakefields results in the photon frequency shift due to variations in the phase velocity [27], where  $v_p$  is given by  $v_p(\xi) \approx c \left[ 1 + \frac{n_e(\xi)}{n_{e0}} \frac{\omega_{p0}^2}{2\omega_0^2} \right]$ ,  $\omega_0$  is the initial laser frequency,  $n_{e0}$  and  $\omega_{p0}$  are the initial plasma electron density and frequency, respectively. The wavelength change of the radiated photons can be estimated by  $\lambda(\tau) \approx \lambda_0 + \tau \Delta v_p(\xi)$ , where  $\Delta v_p(\xi) \approx \lambda_0 \frac{\partial}{\partial \xi} v_p(\xi)$  is the difference of  $v_p(\xi)$  between two adjacent phase peaks. Then,

one can obtain

$$\lambda \approx \lambda_0 + c\tau\lambda_0 \frac{n_{e0}}{2n_c} g(\xi), \quad (1)$$

where  $g(\xi) = \frac{\partial}{\partial \xi} \frac{n_e(\xi)}{n_{e0}}$  is the plasma density gradient,  $\frac{n_e(\xi)}{n_{e0}} = 1 + k_p^{-2} \frac{\partial^2 \phi}{\partial \xi^2}$  is the normalized density perturbation, and  $c\tau$  is the interaction distance. In the short pulse limit when  $|\phi| \ll 1$ , there is [33,34]  $\phi(\xi) \approx \frac{k_p}{2} \int_{\xi}^0 a_L^2(\xi') \sin[k_p(\xi' - \xi)] d\xi'$ , where  $a_L$  is the laser pulse envelope,  $\frac{\partial \phi}{\partial \xi} = 0$  and  $\phi = 0$  at the front ( $\xi \geq 0$ ) of the laser pulse are the boundary conditions. For a given pulse profile  $a_L = a_0 \sin^2(\pi\xi/L)$  for  $-L \leq \xi \leq 0$  and  $a_L = 0$  otherwise, for example, one can obtain  $\phi(\xi) \approx \left(\frac{a_0 k_p L}{16\pi}\right)^2 \left[12 \left(\frac{\pi\xi}{L}\right)^2 + 8\cos\frac{2\pi\xi}{L} - \frac{1}{2}\cos\frac{4\pi\xi}{L} - \frac{15}{2}\right]$ . Therefore,  $g(\xi)$  can be estimated by  $g(\xi) \approx a_0^2 \frac{\pi}{4L} \left(\sin\frac{2\pi\xi}{L} - \frac{1}{2}\sin\frac{4\pi\xi}{L}\right)$ . This gives  $g(\xi) > 0$  in the region of  $-L \leq \xi \leq -L/2$ , where the laser pulse will undergo significant wavelength redshift or frequency downshift. If we assume an average density gradient of  $\bar{g}(\xi) \sim 4\mu m^{-1}$  for the case presented here when  $a_0 > 1$ , the wavelength modulated can be as high as  $10\lambda_0$  over an interaction distance of 1.5mm. It should be pointed out that the above theory only describes qualitatively the frequency modulation due to wakefield excitation. For the quantitative description for LG pulses, the self-consistent three-dimensional (3D) numerical simulation is necessary.

### III. Three-Dimensional Simulation Results

To investigate the development of mid-IR few-cycle twisted pulses, we have carried out fully 3D particle-in-cell (PIC) simulations with the EPOCH code [37]. The size of the simulation box is  $70\mu m(x) \times 120\mu m(y) \times 120\mu m(z)$  with the cells of  $2450 \times 600 \times 600$ , sampled by four macro-particles per cell. The incident linearly-polarized laser pulse has a LG profile of

$$\begin{aligned} \mathbf{a}(\text{LG}_p^l) = & a_0 C_p^l \frac{\sigma_0}{\sigma(x)} \left(\frac{\sqrt{2}r}{\sigma(x)}\right)^l L_p^l \left(\frac{2r^2}{\sigma^2(x)}\right) \exp\left(-\frac{r^2}{\sigma^2(x)}\right) \exp(il\varphi) \exp\left(i\frac{kr^2x}{2(x^2+z_R^2)}\right) \\ & \times \exp\left[-i(l+2p+1)\arctan\frac{x}{z_R}\right] \exp[i(kx - \omega_0 t + \psi_0)] \sin^2(\pi t/\tau_0) \mathbf{e}_y, \end{aligned} \quad (2)$$

where  $a_0 = 3$  is the normalized laser amplitude (intensity  $\sim 10^{19}$  W/cm<sup>2</sup>), with  $\lambda_0 = 1\mu m$  wavelength,

$\tau_0 = 40\text{fs}$  duration and  $\sim 3.1\text{J}$  pulse energy.  $C_p^l$  is the normalizing constant with a low-order  $(1, 0)$   $\text{LG}_0^1$  mode of  $l = 1$  and  $p = 0$ ,  $L_p^l$  is the Laguerre polynomial,  $\varphi \in [0, 2\pi]$  is the azimuthal angle,  $(l + 2p + 1)\arctan\frac{x}{Z_R}$  is the Gouy phase,  $Z_R = \frac{\pi\sigma_0^2}{\lambda_0}$  is the Rayleigh length,  $\sigma(x) = \sigma_0\sqrt{1 + \left(\frac{x}{Z_R}\right)^2}$  is the beam radius, and  $\psi_0$  is the initial phase. Such laser pulses can be produced in several techniques [12,38,39], which have been extensively used to investigate relativistic laser-plasma interactions [40-44].

Figure 2(a-c) presents the distributions of the electron density and transverse electric field at different longitudinal positions along the plasma channel. In contrast to the wake driven by normal Gaussian laser pulses, the wake driven by the LG laser pulse exhibits a donut-like structure with an off-axis hollow density cavity. Along the channel axis, a density up-ramp is introduced at the beginning to guide the laser pulse propagation into the plasma channel. Within this region there is no obvious frequency downshift in the drive pulse, as shown in Figs. 2(a) and 2(d). After a sufficient propagation distance, the laser pulse undergoes both relativistic self-compression and self-focusing, as shown in Fig. 2(b). As a result, the peak laser intensity is enhanced and the density bubble is enlarged, which in turn enhances the relativistic effects and density perturbation. The corresponding frequency spectrum of the laser pulse, shown in Fig. 2(d), illustrates details of the pulse evolution. The spectrum has two main peaks, which result from the photon frequency modulation associated with the plasma density variation. Frequency downshift develops when  $\frac{\partial n_e}{\partial \xi} > 0$  and frequency upshift when  $\frac{\partial n_e}{\partial \xi} < 0$ . The peak of the laser pulse experiences frequency downshift due to the sharp density rise via wakefield excitation, which is mainly responsible for the highest spectral peak at the wavelength  $\sim 1.5\mu\text{m}$ , while the second spectral peak mostly come from its leading edge. The laser pulse peak then experiences strong frequency downshift with very low-frequency components close to  $\omega_p$ . The radiated infrared photons are rapidly slipped back relative to the bubble front due to the group velocity dispersion [ $v_g \approx c(1 - \frac{\omega_p^2}{2\omega^2})$ ] and are trapped inside the bubble. It is interesting to note that there is no electron injection

observed in the bubble cavity due to the relatively low plasma density in our case. This is beneficial for infrared photon trapping, and thus acts as an effective optical container for frequency downshifting conversion. Finally, intense mid-IR pulses are produced with a high energy conversion efficiency of 4.8% (energy  $\sim 150$  mJ) at a long-wavelength spectral range above  $7 \mu\text{m}$ . The output pulse is less than two cycles. For the example illustrated in the inset of Fig. 2(d), the duration is near one optical period at the full width at half maximum. The central wavelength of this pulse is about  $12 \mu\text{m}$  with a peak power of  $\sim 1\text{TW}$  and normalized field amplitude  $a = \frac{eE}{m_e\omega c} \sim 3$ . The transverse distribution of the mid-IR pulse shows a typical LG mode structure, as shown in the inset of Fig. 2(c).

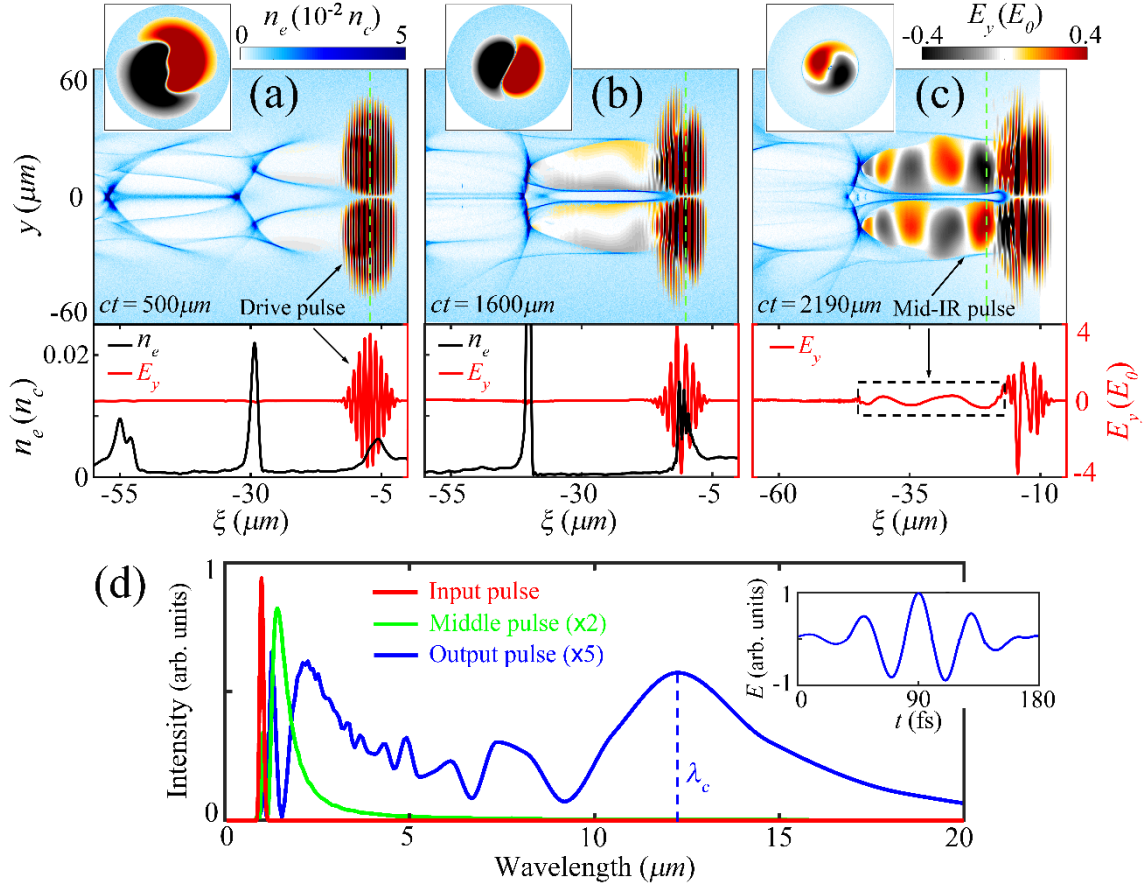


**FIG. 2.** Generation of relativistic mid-IR twisted pulses. (a-c) Distributions of the plasma density ( $n_e$ ) and the transverse electric field ( $E_y$ ) in the  $\xi - y$  plane, and their longitudinal distributions at the transverse position of  $(y, z) = (\sqrt{2}\sigma_0/2, 0)$ . In (a), the laser pulse front has just reached the end of the density up-ramp. In (b), the laser pulse front has reached  $x \approx 1595 \mu\text{m}$ , where the frequency downshift is still relatively small. In (c), the laser pulse front has reached the end of the density down-ramp, where the plasma bubble has been filled with the mid-IR pulse. The upper insets in

(a-c) show the transverse slices of  $E_y$  in the  $y$ - $z$  plane, and the green dashed lines plot their corresponding longitudinal positions. Here, the electric field and electron density are normalized to  $E_0 = m_e c \omega_0 / e$  and  $n_c$ , respectively. (d) Spectral distribution of the modulated pulses, where the red line, green line, and blue line corresponding to the time in (a), (b), and (c), respectively. The inset shows the temporal waveform of the electric field of the infrared pulse at the central wavelength  $\lambda_c \approx 12 \mu m$ . The drive LG laser pulse is with topological charge  $l = 1$ .

The robustness of this mechanism is confirmed by using different plasma parameters. Here, we investigate the effects of two main factors, the plasma plateau and down-ramp, on the mid-IR pulse generation. The up-ramp only serves as an entrance to guide the drive laser propagation in the plasma and the frequency downshift in this region is negligible. We first consider the effect of  $L_p$  on the mid-IR pulse generation. Figure 3(a) shows that a long plateau is helpful in generating intense mid-IR pulses, allowing a long interaction time for frequency downshift and broadening, which agrees well with our theoretical model  $\Delta\lambda/\lambda_0 \propto c\tau n_0 g(\xi)$ . However, beyond an optimum  $L_p \approx 1750 \mu m$  the mid-IR pulse attenuates due to pump depletion and absorption of the laser energy in plasma.

In the region of the down-ramp, the bubble size ( $l_w \approx \sqrt{a_0} \lambda_p \propto \sqrt{a_0/n_e}$ ) tends to be elongated due to a rapid decrease of  $n_e$  whilst there is a relatively small change in  $a_0$ , so that it can accommodate more photons to form long-wave pulses. This results in the increase of the wavelength, energy and duration of the infrared pulse with  $L_f$ . However, further increases of  $L_f$  will lead to pulse attenuation due to absorption and a small bubble size change in an extremely long down-ramp with a gentle change of  $n_e$ . As shown in Fig. 3(b), a moderate-to-long  $L_f$  is beneficial for long-wave infrared pulse generation. Therefore, the plasma down-ramp not only acts as an exit to export the infrared pulse from the plasma, but also plays a role in tuning the output parameters.

The background plasma density also plays an important role on the mid-IR pulse generation, enhancing its tunability. When the plasma density  $n_0$  is increased, sharper density gradients  $g(\xi)$  are formed, making it



easy to modulate the photon frequency (wavelength) in a short interaction distance  $c\tau$ , since  $\Delta\lambda/\lambda_0 \propto c\tau n_0 g(\xi)$ . This is verified by the simulation results shown in Fig. 3(c). However, it should be noted that if the plasma density is too high, the drive laser may be unable to excite a sufficiently large bubble to accommodate the long-wavelength infrared photons. High density plasma also leads to rapid depletion and attenuation of the laser pulse.

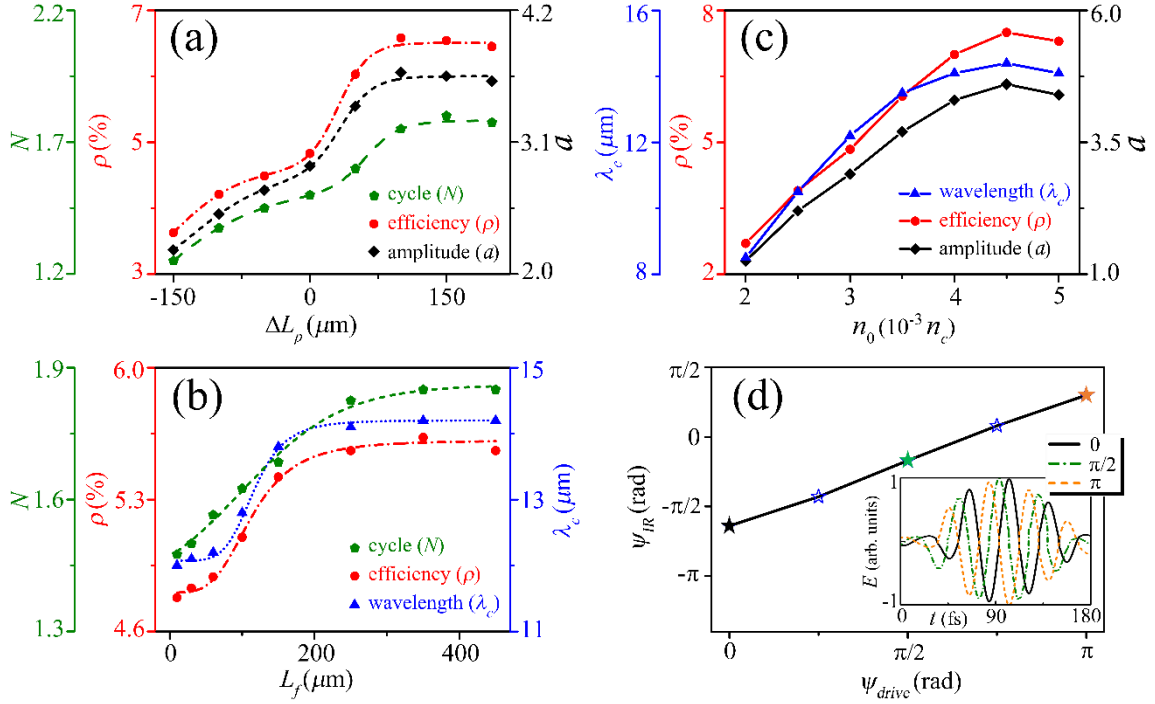


**FIG. 3.** Parameters and phase locking of the twisted mid-IR pulses. (a) Effect of the plasma plateau length  $L_p$  on the optical cycle, energy conversion efficiency and electric field amplitude of the output mid-IR pulse, where  $\Delta L_p = L_p - L_{p0}$  is the change of plasma plateau length relative to the initial plateau length ( $L_{p0} = 1650 \mu\text{m}$ ) shown in Fig. 1(c), keeping all other parameters unchanged. (b) Effect of the density down-ramp length  $L_f$  on the optical cycle, energy conversion efficiency and central wavelength of the output mid-IR pulse, while keeping all other parameters unchanged. (c) Effect of the background plasma density  $n_0$  on the output mid-IR pulse, while keeping fixed  $n_0 L_p = 4.95 n_c \mu\text{m}$ , where the drive laser pulse, and the length of density up- and down-ramps are unchanged. (d) The CEP dependence of the output mid-IR pulse on the drive pulse for the case presented in Fig. 2. The inset plots the waveform of the  $\lambda_c \approx 12 \mu\text{m}$  infrared pulse for three different initial phases ( $\psi_{\text{drive}} = 0, \pi/2, \text{ and } \pi$ ) of the drive laser pulse.

Since the generated mid-IR pulse is only of a few-cycle duration, it is interesting to examine its CEP [45]. The CEP is known to play a significant role in laser-matter interactions with few-cycle pulses, for

example, attosecond pulse generation [23]. Figure 3(d) shows that the CEP of the output long-wavelength pulse is locked to that of the drive pulse in our scheme. The change in the pulse CEP is caused by the difference between the group velocity ( $v_g$ ) and phase velocity ( $v_p$ ) of light propagating in plasma. The phase shift between the infrared pulse and the drive pulse can be approximately estimated by  $\Delta\psi \approx \int_0^{d/c} \frac{(v_p - v_g)}{c} \omega_{IR}(t) dt \approx \int_0^{d/c} \frac{n_e(t)}{n_c} \frac{\omega_0^2}{\omega_{IR}(t)} dt$ , where  $\omega_{IR}(t)$  is the infrared photon frequency, and  $d$  is the plasma length. This indicates that the CEP variation of the infrared pulse will be fixed for a given plasma, because the phase modulation caused by the laser pulse propagating in the plasma is fixed. This leads to a nearly linear relationship between the phases of the infrared pulse and the drive pulse, as seen in Fig. 3(d). Therefore, the CEP of the infrared pulse is controlled by the drive pulse, making it possible to control or measure the CEP in experiments.

#### IV. Discussion and Conclusion

We now discuss the advantage of this scheme for generating high-intensity mid-IR light pulses with different topological charge  $l$  that is directly associated with the OAM states of photons [1,46], i.e., each photon can carry OAMs of  $l\hbar$ . The increase of the topological charge of a light beam typically requires a more complex optical mode converter, which is technically challenging. It is also difficult to generate high-intensity light pulse with a wavelength beyond  $5\mu\text{m}$  through the conventional optical elements, because they commonly suffer from optical breakdown damage with limited wavelength bandwidth and low power carrying capability. In our scheme, high-intensity TW-level mid-IR pulses can be generated with no damage limitation in plasma. Moreover, the topological charge of the twisted mid-IR pulses can be controlled by the drive laser pulse without the need of additional complex optical devices, as illustrated both in Figs. 2 and 4, where the drive LG laser pulses have  $l = 1$  and  $2$ , respectively. Although two drive laser pulses have different topological structures, this does not significantly affect the performance of the mid-IR optical

vortex pulse generation scheme, where both of them show a quite similar spectrum. This thus provides an approach towards the generation of high-power, high-intensity, vortex-stabilized, few-cycle mid-IR pulses.

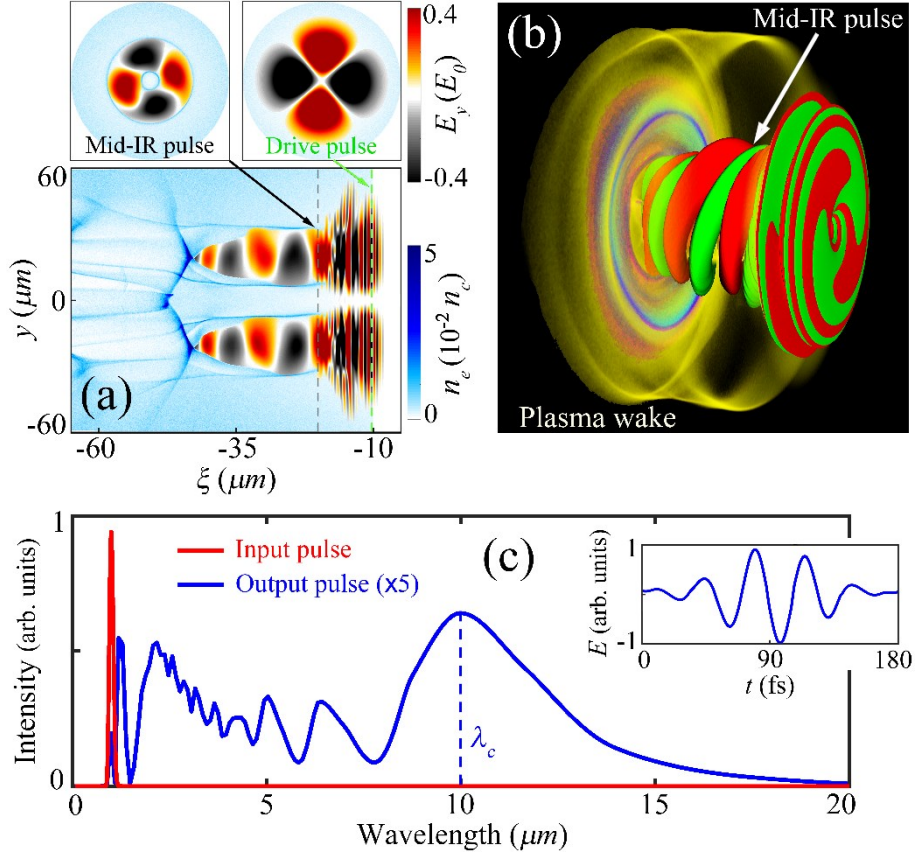


**FIG. 4.** Conversion from a drive laser pulse with  $l = 2$  to twisted mid-IR pulses using a plasma photon decelerator. Distributions of mid-IR pulses in the  $\xi - y$  plane (a) and in 3D view (b). Here the topological charge of the drive laser pulse is changed from  $l = 1$  to 2 for the case presented in Fig. 2, but all other parameters are unchanged. The insets in (a) presents the transverse electric field slices of the drive pulse and the mid-IR pulse in the  $y - z$  plane. (c) Spectral distributions of the input drive pulse and the output infrared pulse. The inset plots the temporal waveform of the electric field of the  $\lambda_c \approx 10 \mu\text{m}$  infrared pulse.

In conclusion, we have demonstrated a promising and practical way to generate TW-class hundred-mJ near-single-cycle mid-IR twisted pulses via photon deceleration in plasma. The generated pulses not only cover a broad spectrum up to  $18 \mu\text{m}$ , but also can reach relativistically high intensities. Furthermore, the output parameters of the mid-IR pulses can be flexibly tuned by the plasma parameters, and the CEP can be locked and controlled by that of the drive pulse. Such light sources, with relativistic high-intensities in the

long-wavelength infrared spectral region, offer many potential applications in high-field physics and ultrafast science.

## Acknowledgements

This work was supported by the National Natural Science Foundation of China (Grant Nos. 11721091, 11775144, and 11975154), the office of Science and Technology, Shanghai Municipal Government (Grant No. 18JC1410700), Science Challenge Project (Grant No. TZ2018005), and EC H2020 EuPRAXIA (Grant No. 653782). X.L.Z. acknowledges support from the China Scholarship Council. The EPOCH code was supported in part by the UK EPSRC (Grant No. EP/G056803/1). All simulations were carried out on the PI supercomputer at Shanghai Jiao Tong University, Tianhe-II supercomputer at the National Supercomputer Center in Guangzhou, and ARCHER supercomputer in Edinburgh. Access to ARCHER has been made via the Plasma HEC Consortium supported by EPSRC (No. EP/R029148/1).

## References

- [1] L. Allen, M. W. Beijersbergen, R. Spreeuw, and J. Woerdman, Orbital angular momentum of light and the transformation of Laguerre-Gaussian laser modes, *Phys. Rev. A* **45**, 8185 (1992).
- [2] A. Mair, A. Vaziri, G. Weihs, and A. Zeilinger, Entanglement of the orbital angular momentum states of photons, *Nature* **412**, 313 (2001).
- [3] G. Molina-Terriza, J. P. Torres, and L. Torner, Twisted photons, *Nat. Phys.* **3**, 305 (2007).
- [4] S. Fürhapter, A. Jesacher, S. Bernet, and M. Ritsch-Marte, Spiral phase contrast imaging in microscopy, *Opt. Express* **13**, 689 (2005).
- [5] M. Padgett and R. Bowman, Tweezers with a twist, *Nat. Photon.* **5**, 343 (2011).
- [6] D. G. Grier, A revolution in optical manipulation, *Nature* **424**, 810 (2003).
- [7] F. Tamburini, B. Thidé, G. Molina-Terriza, and G. Anzolin, Twisting of light around rotating black holes, *Nat. Phys.* **7**, 195 (2011).
- [8] A. M. Yao and M. J. Padgett, Orbital angular momentum: origins, behavior and applications, *Adv. Opt. Photon.* **3**, 161 (2011).
- [9] M. W. Beijersbergen, L. Allen, H. Van der Veen, and J. Woerdman, Astigmatic laser mode converters and transfer of orbital angular momentum, *Opt. Commun.* **96**, 123 (1993).

- [10] G. Gariepy, J. Leach, K. T. Kim, T. J. Hammond, E. Frumker, R. W. Boyd, and P. B. Corkum, Creating High-Harmonic Beams with Controlled Orbital Angular Momentum, *Phys. Rev. Lett.* **113**, 153901 (2014).
- [11] R. Généaux, A. Camper, T. Auguste, O. Gobert, J. Caillat, R. Taïeb, and T. Ruchon, Synthesis and characterization of attosecond light vortices in the extreme ultraviolet, *Nat. Commun.* **7**, 12583 (2016).
- [12] A. Leblanc, A. Denoeud, L. Chopineau, G. Mennerat, P. Martin, and F. Quéré, Plasma holograms for ultrahigh-intensity optics, *Nat. Phys.* **13**, 440 (2017).
- [13] G. A. Mourou, T. Tajima, and S. V. Bulanov, Optics in the relativistic regime, *Rev. Mod. Phys.* **78**, 309 (2006).
- [14] X.-L. Zhu, T.-P. Yu, Z.-M. Sheng, Y. Yin, I. C. E. Turcu, and A. Pukhov, Dense GeV electron-positron pairs generated by lasers in near-critical-density plasmas, *Nat. Commun.* **7**, 13686 (2016).
- [15] X.-L. Zhu, T.-P. Yu, M. Chen, S.-M. Weng, and Z.-M. Sheng, Generation of GeV positron and  $\gamma$ -photon beams with controllable angular momentum by intense lasers, *New J. Phys.* **20**, 083013 (2018).
- [16] A. Schliesser, N. Picqué, and T. W. Hänsch, Mid-infrared frequency combs, *Nat. Photon.* **6**, 440 (2012).
- [17] I. Pupeza, D. Sánchez, J. Zhang, N. Lilienfein, M. Seidel, N. Karpowicz, T. Paasch-Colberg, I. Znakovskaya, M. Pescher, W. Schweinberger, V. Pervak, E. Fill, O. Pronin, Z. Wei, F. Krausz, A. Apolonski, and J. Biegert, High-power sub-two-cycle mid-infrared pulses at 100 MHz repetition rate, *Nat. Photon.* **9**, 721 (2015).
- [18] B. Wolter, M. G. Pullen, M. Baudisch, M. Sclafani, M. Hemmer, A. Senftleben, C. D. Schröter, J. Ullrich, R. Moshhammer, and J. Biegert, Strong-Field Physics with Mid-IR Fields, *Phys. Rev. X* **5**, 021034 (2015).
- [19] T. Popmintchev, M.-C. Chen, D. Popmintchev, P. Arpin, S. Brown, S. Ališauskas, G. Andriukaitis, T. Balčiūnas, O. D. Mücke, A. Pugzlys, A. Baltuška, B. Shim, S. E. Schrauth, A. Gaeta, C. Hernández-García, L. Plaja, A. Becker, A. Jaron-Becker, M. M. Murnane, and H. C. Kapteyn, Bright Coherent Ultrahigh Harmonics in the keV X-ray Regime from Mid-Infrared Femtosecond Lasers, *Science* **336**, 1287 (2012).
- [20] J. Weisshaupt, V. Juvé, M. Holtz, S. Ku, M. Woerner, T. Elsaesser, S. Ališauskas, A. Pugzlys, and A. Baltuška, High-brightness table-top hard X-ray source driven by sub-100-femtosecond mid-infrared pulses, *Nat. Photon.* **8**, 927 (2014).
- [21] C. R. Petersen, U. Møller, I. Kubat, B. Zhou, S. Dupont, J. Ramsay, T. Benson, S. Sujecki, N. Abdel-

- Moneim, Z. Tang, D. Furniss, A. Seddon, and O. Bang, Mid-infrared supercontinuum covering the 1.4–13.3  $\mu\text{m}$  molecular fingerprint region using ultra-high NA chalcogenide step-index fibre, *Nat. Photon.* **8**, 830 (2014).
- [22] C. I. Blaga, J. Xu, A. D. DiChiara, E. Sistrunk, K. Zhang, P. Agostini, T. A. Miller, L. F. DiMauro, and C. D. Lin, Imaging ultrafast molecular dynamics with laser-induced electron diffraction, *Nature* **483**, 194 (2012).
- [23] F. Krausz and M. Ivanov, Attosecond physics, *Rev. Mod. Phys.* **81**, 163 (2009).
- [24] P. Colosimo, G. Doumy, C. I. Blaga, J. Wheeler, C. Hauri, F. Catoire, J. Tate, R. Chirla, A. M. March, G. G. Paulus, H. G. Muller, P. Agostini, and L. F. DiMauro, Scaling strong-field interactions towards the classical limit, *Nat. Phys.* **4**, 386 (2008).
- [25] M. Zürch, C. Kern, P. Hansinger, A. Dreischuh, and C. Spielmann, Strong-field physics with singular light beams, *Nat. Phys.* **8**, 743 (2012).
- [26] A. J. Gonsalves, K. Nakamura, J. Daniels, C. Benedetti, C. Pieronek, T. C. H. de Raadt, S. Steinke, J. H. Bin, S. S. Bulanov, J. van Tilborg, C. G. R. Geddes, C. B. Schroeder, C. Tóth, E. Esarey, K. Swanson, L. Fan-Chiang, G. Bagdasarov, N. Bobrova, V. Gasilov, G. Korn, P. Sasorov, and W. P. Leemans, Petawatt Laser Guiding and Electron Beam Acceleration to 8 GeV in a Laser-Heated Capillary Discharge Waveguide, *Phys. Rev. Lett.* **122**, 084801 (2019).
- [27] E. Esarey, C. Schroeder, and W. Leemans, Physics of laser-driven plasma-based electron accelerators, *Rev. Mod. Phys.* **81**, 1229 (2009).
- [28] S. C. Wilks, J. M. Dawson, W. B. Mori, T. Katsouleas, and M. E. Jones, Photon accelerator, *Phys. Rev. Lett.* **62**, 2600 (1989).
- [29] F. S. Tsung, C. Ren, L. O. Silva, W. B. Mori, and T. Katsouleas, Generation of ultra-intense single-cycle laser pulses by using photon deceleration, *Proc. Natl. Acad. Sci. USA* **99**, 29 (2002).
- [30] D. F. Gordon, B. Hafizi, R. F. Hubbard, J. R. Peñano, P. Sprangle, and A. Ting, Asymmetric Self-Phase Modulation and Compression of Short Laser Pulses in Plasma Channels, *Phys. Rev. Lett.* **90**, 215001 (2003).
- [31] W. Zhu, J. P. Palastro, and T. M. Antonsen, Pulsed mid-infrared radiation from spectral broadening in laser wakefield simulations, *Phys. Plasmas* **20**, 073103 (2013).
- [32] Z. Nie, C.-H. Pai, J. Hua, C. Zhang, Y. Wu, Y. Wan, F. Li, J. Zhang, Z. Cheng, Q. Su, S. Liu, Y. Ma, X. Ning, Y. He, W. Lu, H.-H. Chu, J. Wang, W. B. Mori, and C. Joshi, Relativistic single-cycle tunable

infrared pulses generated from a tailored plasma density structure, *Nat. Photon.* **12**, 489 (2018).

- [33] P. Sprangle, E. Esarey, and A. Ting, Nonlinear theory of intense laser-plasma interactions, *Phys. Rev. Lett.* **64**, 2011 (1990).
- [34] E. Esarey, A. Ting, and P. Sprangle, Frequency shifts induced in laser pulses by plasma waves, *Phys. Rev. A* **42**, 3526 (1990).
- [35] Z.-M. Sheng, J.-X. Ma, Z.-Z. Xu, and W. Yu, Effect of an electron plasma wave on the propagation of an ultrashort laser pulse, *J. Opt. Soc. Am. B* **10**, 122 (1993).
- [36] W. B. Mori, The physics of the nonlinear optics of plasmas at relativistic intensities for short-pulse lasers, *IEEE J. Quantum Electron.* **33**, 1942 (1997).
- [37] T. D. Arber, K. Bennett, C. S. Brady, A. Lawrence-Douglas, M. G. Ramsay, N. J. Sircombe, P. Gillies, R. G. Evans, H. Schmitz, A. R. Bell, and C. P. Ridgers, Contemporary particle-in-cell approach to laser-plasma modelling, *Plasma Phys. Control. Fusion* **57**, 113001 (2015).
- [38] Y. Shi, B. Shen, L. Zhang, X. Zhang, W. Wang, and Z. Xu, Light Fan Driven by a Relativistic Laser Pulse, *Phys. Rev. Lett.* **112**, 235001 (2014).
- [39] C. Brabetz, S. Busold, T. Cowan, O. Deppert, D. Jahn, O. Kester, M. Roth, D. Schumacher, and V. Bagnoud, Laser-driven ion acceleration with hollow laser beams, *Phys. Plasmas* **22**, 013105 (2015).
- [40] A. Denoeud, L. Chopineau, A. Leblanc, and F. Quéré, Interaction of Ultraintense Laser Vortices with Plasma Mirrors, *Phys. Rev. Lett.* **118**, 033902 (2017).
- [41] J. Vieira and J. T. Mendonça, Nonlinear Laser Driven Donut Wakefields for Positron and Electron Acceleration, *Phys. Rev. Lett.* **112**, 215001 (2014).
- [42] G.-B. Zhang, M. Chen, J. Luo, M. Zeng, T. Yuan, J.-Y. Yu, Y.-Y. Ma, T.-P. Yu, L.-L. Yu, S.-M. Weng, and Z.-M. Sheng, Acceleration of on-axis and ring-shaped electron beams in wakefields driven by Laguerre-Gaussian pulses, *J. Appl. Phys.* **119**, 103101 (2016).
- [43] X.-L. Zhu, M. Chen, T.-P. Yu, S.-M. Weng, L.-X. Hu, P. McKenna, and Z.-M. Sheng, Bright attosecond  $\gamma$ -ray pulses from nonlinear Compton scattering with laser-illuminated compound targets, *Appl. Phys. Lett.* **112**, 174102 (2018).
- [44] L.-X. Hu, T.-P. Yu, Z.-M. Sheng, J. Vieira, D.-B. Zou, Y. Yin, P. McKenna, and F.-Q. Shao, Attosecond electron bunches from a nanofiber driven by Laguerre-Gaussian laser pulses, *Sci. Rep.* **8**, 7282 (2018).
- [45] T. Wittmann, B. Horvath, W. Helml, M. G. Schätzel, X. Gu, A. L. Cavalieri, G. G. Paulus, and R. Kienberger, Single-shot carrier-envelope phase measurement of few-cycle laser pulses, *Nat. Phys.* **5**,

357 (2009).

- [46] A. T. O'Neil, I. MacVicar, L. Allen, and M. J. Padgett, Intrinsic and Extrinsic Nature of the Orbital Angular Momentum of a Light Beam, *Phys. Rev. Lett.* **88**, 053601 (2002).